Available online at www.sciencedirect.com
SCIENCE DIRECT®
Pergamon
Cement and Concrete Research 34 (2004) 1845–1852
CEMENT AND CONCRETE RESEARCH

Polytypes and polymorphs in the related Friedel's salt $[Ca_2Al(OH)_6]^+[X{\cdot}2H_2O]^-$ halide series

G. Renaudin[a], J.-P. Rapin[b], E. Elkaim[c], M. François[b,*]

[a]Laboratoire de Cristallographie, Université de Genève, 24 quai Ernest Ansermet, CH-1211, Geneva 4, Switzerland
[b]Laboratoire de Chimie du Solide Minéral—UMR 7555, Université Henri Poincaré, Nancy I, F-54506, Vandoeuvre-les-Nancy, France
[c]Laboratoire LURE, Bat 209D, Centre Universitaire Paris Sud, BP 34, F-91898 Orsay Cedex, France

Received 6 May 2003; accepted 22 January 2004

Abstract

Seven substituted Friedel's salt samples from the solid solution $[Ca_2Al(OH)_6]^+[Cl_{1-x}Br_x{\cdot}2H_2O]^-$ were synthesised by hydrothermal synthesis ($x=0$, 0.23, 0.44, 0.57, 0.66, 0.78, and 1.0). These compounds, belonging to the layered double hydroxide family, present a structural phase transition from the rhombohedral HT-polymorph to the monoclinic LT-polymorph. The transition has been detected by differential scanning calorimetry and then characterized by X-ray diffraction. Rietveld analyses have been used to evaluate the structural modifications. The transition temperature is related to the ionic radius and the hydration enthalpy of the halide. As one goes from heavy to light halide, there is a strengthening of the water to halide hydrogen bonds that favours the LT-polymorph (with four short halide-to-water bonds) at the expense of the HT-polymorph (with six larger halide-to-water bonds) implying an increase of the transition temperature. The study has been enlarged to the analogous iodide compound.

Keywords: Crystal structure; X-ray diffraction; Thermal analysis; Structural transition, Friedel's salts

1. Introduction

The Friedel's salt $Ca_2Al(OH)_6{\cdot}Cl{\cdot}2H_2O$ belongs to the AFm phases (a family of hydrated compounds found in cement pastes), a subgroup of the wide family of layered double hydroxide (LDH) compounds. The AFm phases are composed of positively charged main layers $[Ca_2Al(OH)_6]^+$, and negatively charged interlayers $[X{\cdot}nH_2O]^-$ where X^- is a mineral anion. We present in this paper a study on the substitution of chloride by bromide in the related Friedel's salt solid solution $[Ca_2Al(OH)_6]^+[Cl_{1-x}Br_x{\cdot}2H_2O]^-$ with $0\le x\le 1$. As the compounds studied are distinguished by the nature of the inserted X halide, they are noticed in the following by AFm-X. Friedel's salt, AFm-Cl, presents a structural phase transition which has been fully characterized by synchrotron powder diffraction data in our previous work [1]. AFm-Cl transforms during cooling at 308 K from a high-temperature phase (HT-polymorph) with rhombohedral symmetry [$R\bar{3}c$, $a=5.744(2)$, $c=46.890(3)$ Å] [2] to a low-temperature phase (LT-polymorph) with monoclinic symmetry [$C2/c$, $a=9.960(4)$, $b=5.7320(2)$, $c=16.268(7)$ Å, $\beta=104.471(2)°$] [1]. The coordination numbers of the Al^{3+} and Ca^{2+} ions in both polymorphs are 6 and 7, respectively. Each Ca^{2+} is approached by a seventh O-atom from a water molecule. The chloride anions, linked by hydrogen bonds, have 10 H-atoms as first neighbours (six from hydroxyl groups and four from water molecules) and 12 O-atoms as second neighbours (six from hydroxyl groups and six from water molecules). It has been shown that the transition is due to an ordering of the hydrogen bonds network around the chloride anion [1]. Our results were in good agreement with a ^{27}Al MAS NMR spectroscopy study [3] that has detected the transition at 307 K for AFm-Cl and the prediction of a dynamic disorder in this compound performed by molecular dynamic modelling [4]. A transition was also detected at 267 K by ^{35}Cl NMR spectroscopy [5] on hydrocalumite, $Ca_{1.96}Al_{1.04}(OH)_6{\cdot}Cl_{0.76}(CO_3)_{0.14}{\cdot}2H_2O$, a natural mineral with composition very close to those of Friedel's salts, but including a weak substitution of chloride by carbonate in the interlayer region. The assumption was then made that the transition temperatures (Ts) depend on the nature of the intercalated

* Corresponding author. Tel.: +33-3-83-68-46-58; fax: +33-3-83-68-46-11.
E-mail address: michel.francois@lcsm.uhp-nancy.fr (M. François).

0008-8846/$ – see front matter © 2004 Elsevier Ltd. All rights reserved.
doi:10.1016/j.cemconres.2004.01.003

halide anion. The aim of this work was to investigate the influence of nature of the halide anions on the temperature-dependent structural transition. Accurate crystallographic data for the HT-polymorphs of AFm-X were available for $X = Cl^-$ [2], $(Cl_{0.5}Br_{0.5})^-$ [6], Br^- [7] and I^- [8] that are 6R, 6R, 3R and 3R polytypes, respectively. Concerning the crystal structure of the LT-polymorph, up to now, accurate crystallographic data were only available for $X = Cl^-$ [1]. We present here the newly observed 6R polytype of AFm-Br on single crystal $[Ca_2Al(OH)_6 \cdot Br \cdot 2H_2O$ compound, $R\bar{3}c$ trigonal space group, $a = 5.763(1)$, $c = 49.108(1)$ Å, $Z = 6$, $R1 = 0.0449$ and $wR2 = 0.0897$], showing that this bromide phase exists with both 3R and 6R polytypes for its HT-polymorph. We report also the new crystallographic data of the LT-polymorphs for $X=(Cl_{0.43}Br_{0.57})^-$ $(Ca_2Al(OH)_6 \cdot Cl_{0.43}Br_{0.57} \cdot 2H_2O$ compound, $C2/c$ monoclinic space group, $a = 9.9899(9)$, $b = 5.7470(6)$, $c = 16.667(2)$ Å and $\beta = 104.095(6)°$, $Z = 4$, $R_{Bragg} = 14.0\%$, $R_f = 10.9\%$ and $\chi^2 = 4.1$) and Br^- $(Ca_2Al(OH)_6 \cdot Br \cdot 2H_2O$ compound, $C2/c$ monoclinic space group, $a = 9.992(1)$, $b = 5.7405(6)$, $c = 16.845(2)$ Å and $\beta = 103.675(7)°$, $Z = 4$, $R_{Bragg} = 19.7\%$, $R_f = 19.1\%$ and $\chi^2 = 22.9$) obtained from Rietveld analyses on X-rays powder patterns. These crystallographic data allow us to study the transition along the solid solution AFm-$Cl_{1-x}Br_x$ (seven samples have been synthesised, with $x = 0$, 0.23, 0.44, 0.57, 0.66, 0.78 and 1.0). Expansion of the study has also been made by studying the transition of the iodide equivalent compound AFm-I that presents the 3R polytype for its HT-polymorph.

2. Experimental

2.1. Sample preparation, chemical and thermal analysis

2.1.1. -AFm-$Cl_{1-x}Br_x$

Seven crystalline samples from the solid solution $[Ca_2Al(OH)_6]^+[Cl_{1-x}Br_x \cdot 2H_2O]^-$ were synthesised by hydrothermal synthesis for various nominal x values ($x = 0.0$, 0.25, 0.4, 0.6, 0.7, 0.8 and 1.0) following the indications given previously [9]. The composition of elements Ca, Al and halides (Cl and Br) are determined by using a microprobe analysis (Cameca SX50) and averaged from measurements on three single crystals extracted from each batch. The Ca/Al ratio was always 2 and the x determined values were successively 0, 0.23, 0.44, 0.57, 0.66, 0.78 and 1.0. Water content is verified by TGA (Setaram TGA92) measurement performed from room temperature to 1000 °C. In each case, the weight losses correspond to the 10 water molecules expressed in the general formula $3CaO \cdot Al_2O_3 \cdot CaX_2 \cdot 10H_2O$. Differential scanning calorimetry (DSC Mettler TA 4000), over a temperature range of 213–773 K and a heating rate of 5 K min^{-1} under a flowing argon atmosphere, was used to determine Ts. The low-temperature region of the DSC curves for the seven samples, showing the endothermic peak of the structural phase transition on heating, are presented in Fig. 1. Ts strongly decreases along the solid solution AFm-$Cl_{1-x}Br_x$ from 309 to 228 K when x increases from 0 (AFm-Cl) to 1 (AFm-Br), respectively.

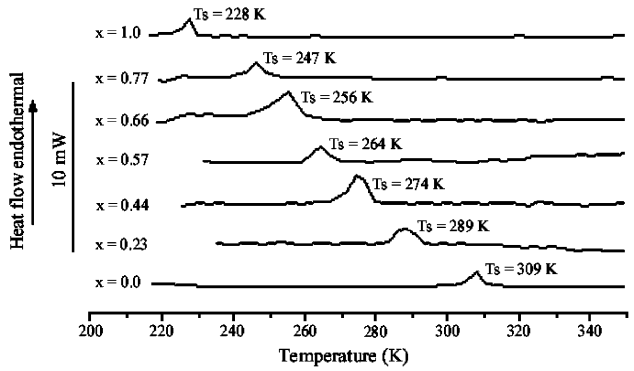

Fig. 1. Low-temperature region of the DSC curves in AFm-$Cl_{1-x}Br_x$ showing the variation of the Ts as a function of x.

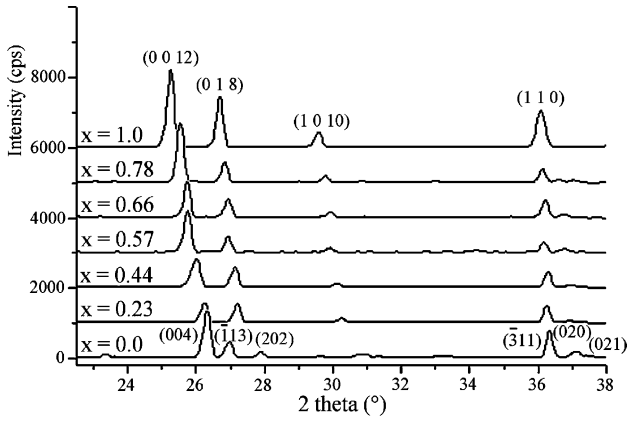

Fig. 2. X-ray powder patterns of samples from the solid solution AFm-$Cl_{1-x}Br_x$ at room temperature ($\lambda = 1.7889$ Å). Miller indices of Bragg peaks are indicated: monoclinic lattice for the sample with $x = 0$ (LT-polymorph) and hexagonal lattice for the six other samples (HT-polymorph).

2.1.2. AFm-I

Powder sample with composition of $[Ca_2Al(OH)_6]^+$ $[I \cdot 2H_2O]^-$ was prepared by anionic exchange from AFm-Cl powder placed in a KI solution (2 M) under magnetic stirring during 15 days as previously indicated [10].

A large part of each preparation was grinded for X-ray powder analysis. AFm-$Cl_{1-x}Br_x$ and AFm-I samples were measured on an INEL CPS 120 diffractometer to verify their purity and crystallinity. The powder patterns were first analysed using the Diffrac-AT program [11], which includes phases identification using the ICDD Powder Diffraction File Database. Fig. 2 shows a selected region of the patterns from the seven samples of the AFm-$Cl_{1-x}Br_x$ solid solution recorded at 293 K. In accordance with the DSC measurements (Fig. 1), we observe the LT-polymorph (monoclinic cell) for the sample AFm-Cl ($x = 0$) and the HT-polymorph

Table 1
Composition (x), lattice parameters and interlamellar distance (d_0) of the rhombohedral HT-polymorph refined from single crystals of the AFm-$Cl_{1-x}Br_x$ solid solution

x	a (Å)	c (Å)	d_0 (Å)	Temperature (K)
0(2)	5.724(1)	46.689(5)	7.782(5)	310
0.23	5.751(2)	47.315(2)	7.885(2)	273
0.44	5.758(1)	47.804(1)	7.967(1)	273
0.57	5.753(1)	48.108(4)	8.018(4)	273
0.66	5.762(2)	48.306(3)	8.051(2)	273
0.78	5.763(1)	48.542(1)	8.090(1)	273
1.0	5.763(1)	49.108(1)	8.185(1)	273

(hexagonal cell) for the six others samples ($0.23 \le x \le 1$). Fig. 2 illustrates the effect on the chloride substitution by larger bromide on the lattice metric. As the value of x increases, the (001) reflections type are shifted towards small angles. On the other hand, shifts are less pronounced for the (110) reflections type, that is related to the rigidity of the metal hydroxide $[Ca_2Al(OH)_6]^+$ main layers, related CdI_2 structure type of the AFm structure.

2.2. Single crystal X-ray diffraction at room temperature

2.2.1. Data collections

Single crystal X-ray diffraction at 293 K has been performed for the AFm-$Cl_{1-x}Br_x$ compounds with $x = 0.23$, 0.44, 0.57, 0.66, 0.78 and 1.0. One single crystal extracted from each batch was mounted on a Kappa CCD diffractometer (Nonius). The lattice parameters were measured for each crystal by recording 20 images in phi-scan mode (2°/min). Cell refinement is performed by using SCALEPACK in HKL program [12]. Table 1 indicates the refined lattice parameters of the hexagonal cells for these samples. The c parameter increases strongly from 46.689 Å for $x = 0$ to 49.108 Å for $x = 1$ and the a parameter undergoes a weak increase from 5.724 Å for $x = 0$ to 5.763 Å for $x = 1$. Fig. 3 shows that the variation of interlamellar distance (d_0) is linearly dependent of the halide radius [13]. The ionic radius used for halide in AFm-$Cl_{1-x}Br_x$ compounds is the weighted sum of Cl^- and Br^- radius. As for the other compositions, we have observed for the $x = 1.0$ compound (AFm-Br), the 6R polytype in contrast with the 3R polytype previously found [7]. Thus, a complete data collection was measured on this single crystal. Data reduction was performed by using SCALEPACK and DENZO in HKL program [12].

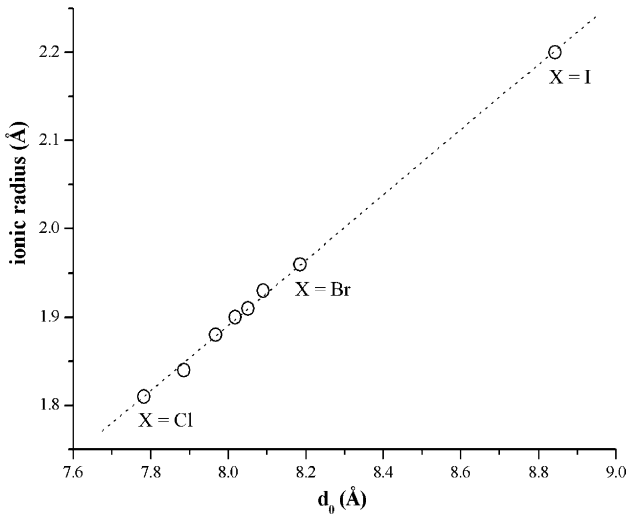

Fig. 3. Interlamellar distance (d_0) as a function of the ionic radius of the inserted halide X^- in the AFm-X series. Linear fit (dotted line) is a guide for the eyes.

2.2.2. Structure analysis

This AFm-Br polytype at room temperature is isotypic to the 6R polytype of AFm-Cl determined at 37 °C [2]. Refinement of the structure was made using SHELXL [14]. The parameters for the data collection are summarized in Table 2. Atomic coordinates and thermal displacement parameters are reported in Table 3. They are comparable with those of AFm-Cl measured at 310 K [2] and AFm-$Cl_{0.5}Br_{0.5}$ measured at room temperature [6]. Selected interatomic distances are reported in Table 4 and comparison with both polytypes of other compounds from the AFm-X series is given.

2.3. X-ray powder diffraction (XRPD) at room and low temperature

2.3.1. Data collections

The LT-polymorph of the compounds AFm-$Cl_{0.43}Br_{0.57}$, AFm-Br and AFm-I were investigated by XRPD. The

Table 2
Refinement and data collection parameters for the 6R polytype of AFm-Br

Compound	$[Ca_2Al(OH)_6]^+[Br{\cdot}2H_2O]^-$
Chemical formula	$AlBrCa_2H_{10}O_8$
Formula weight (g mol^{-1})	325.13
Temperature (K)	293(2)
Wavelength (Å)	0.56050
Space group	$R\bar{3}c$
Unit cell dimensions (Å)	$a = 5.763(1)$, $c = 49.108(1)$
Volume ($Å^3$)	1412.5(3)
Z/calculated density (g cm^{-3})	6/2.293
Absorption coefficient (mm^{-1})	2.940
F(000)	972
Crystal form/color	Hexagonal/transparent
Crystal size (mm)	0.110 × 0.090 × 0.030
Theta range for data collection	$1.46° < \theta < 18.56°$
Diffraction reflections limits	$0 < h < 6$; $-5 < k < 0$; $-53 < l < 54$
Reflections collected	414
Reflections independent	248
Refinement method	Least square on F^2
Number of data/restraints	209/2
Parameters	26
Goodness of fit on F^2	1.126
Final R indices [$I > 2\sigma(I)$]	R1 = 0.0356
Final R indices on whole data	R1 = 0.0450. wR2 = 0.0877
Largest difference peak and hole	0.383 and −0.743 e^- .$Å^3$

Table 3
Atomic coordinates and thermal displacement parameters for the 6R polytype of AFm-Br refined on single crystal [$Ca_2Al(OH)_6 \cdot Br \cdot 2H_2O$ compound, $R\bar{3}c$ trigonal space group, $a = 5.763(1)$, $c = 49.108(1)$ Å, $Z = 6$]

Atom	Site	x	y	z	U_{eq}[a] ($Å^2 \times 10^3$)	Occupancy
Al	6*b*	0	0	0	12.7(8)	1
Ca	12*c*	2/3	1/3	0.98810(3)	14.9(5)	1
Br	6*a*	0	0	1/4	51.9(6)	1
O_H	36*f*	0.0560(6)	0.3066(6)	−0.02027(7)	15.2(8)	1
H	36*f*	0.130(9)	0.332(9)	−0.0370(5)	18(−)	1
O_W	12*c*	2/3	1/3	0.9377(2)	51(2)	1
H_W	36*f*	0.58(2)	0.42(2)	0.930(2)	61(−)	2/3

[a] U_{eq} is one third of the trace of the matrix U_{ij}. $U_{eq} = 1/3(\Sigma_i \Sigma_j U_{ij} a_i * a_j * a_i a_j)$.

samples AFm-$Cl_{0.43}Br_{0.57}$ and AFm-I were studied by using a Huber Guinier Diffractometer System 600 with a monochromatic [Ge(111)] $CuK_{\alpha 1}$ radiation. The diffractometer was equipped with a closed-cycle helium Helix Model 22 Refrigerator [15]. The finely ground powders (grain size ≈ 10 μm) were placed between two Millar foils. The compound AFm-Br was investigated by synchrotron radiation using the WDIF4C diffractometer on the DW22 line of LURE [16]. The powder was finely crushed (grain size = 1–10 μm) and introduced in a Lindeman tube ($\Phi = 0.5$ mm). Rotation of the sample around the capillary axis was applied to reduce preferred orientation problem inherent to such layered compounds. Data were recorded in Debye–Scherrer geometry. A low-temperature attachment [17] based on blowing cold nitrogen gas was used. Two spectra were recorded for these three samples, one at room temperature and the other below Ts. The experimental parameters used for the measurements are summarized in Table 5.

2.3.2. Structures analysis

The atomic positional parameters for the HT and LT-polymorphs were refined from the patterns by using the Rietveld method with the program Fullprof.2k [18]. The HT powder patterns of AFm-$Cl_{0.43}Br_{0.57}$ and AFm-Br are indexed in the hexagonal lattices $a = 5.7537(4)$, $c = 48.108(4)$ Å and $a = 5.763(1)$, $c = 49.108(2)$ Å, respectively, thus corresponding to the 6R polytype. The atomic starting parameters used for the HT-polymorphs ($R\bar{3}c$, Al in 6*b*, X^- in 6*a*, Ca and H_2O in 12*c*, OH in 36*f*) were those reported from single crystal X-ray diffraction study on AFm-Cl [2]. Rietveld refinements on the room temperature data are used to check the quality of our polycrystalline samples. Results were in good agreement with previous single crystal studies. The atomic starting parameters used for the monoclinic LT-polymorphs ($C2/c$, Al in 4*a*, X^- in 4*e*, Ca, O_W, O_H1, O_H2 and O_H3 in 8*f*) were taken from the synchrotron study on AFm-Cl [1]. The AFm-Br sample contains large amounts of impurities (calcite, gibbsite, bayerite and ice) that decreases the accuracy of the result concerning this phase, while the AFm-$Cl_{0.43}Br_{0.57}$ sample can be considered as a pure compound. For the AFm-I sample, only the pattern recorded at room temperature with the HT-polymorph has been refined using $R\bar{3}$ space group (Al in 3*a*, X^- in 3*b*, Ca and H_2O in 6*c*, OH in 18*f*) as initial parameters [8]. Quality of the low-temperature data for the AFm-I sample was not good enough to solve ab initio the structure of the LT-polymorph in the presumably triclinic $P\bar{1}$ space group. The LT pattern of AFm-I sample can be indexed in the triclinic lattice $a = 9.337(1)$, $b = 9.545(1)$, $c = 9.516(1)$ Å, $\alpha = 35.180(4)°$, $\beta = 35.779(4)°$, $\gamma = 35.747(4)°$. The temperature of transition for the AFm-I sample has been detected by XRPD as a function of temperature around 133 K. The following 33 parameters were allowed to vary for the refinement of the LT-polymorph of the AFm-$Cl_{0.43}Br_{0.57}$ phase: 1 scale, 5 profile, 4 cell, 1

Table 4
Selected interatomic distances (Å) for both 3R and 6R polytypes of the HT-polymorphs in the AFm-X series

Anion →	X = I	X = Br		X = $Cl_{0.5}Br_{0.5}$	X = Cl
Polytype →	3R [8]	3R [7]	6R	6R [6]	6R [2]
Temperature →	293 K	293 K	293 K	293 K	310 K
Al–6O_H	1.910(3)	1.909(3)	1.910(4)	1.911(2)	1.905(3)
Ca–3O_H	2.369(3)	2.359(3)	2.361(4)	2.357(2)	2.352(3)
–3O_H	2.454(4)	2.454(3)	2.458(4)	2.461(2)	2.457(5)
–O_W	2.440(8)	2.465(5)	2.477(8)	2.491(5)	2.497(7)
X–6O_W	3.621(2)	3.482(2)	3.483(2)	3.450(1)	3.410(1)
–6O_H	3.911(3)	3.615(3)	3.624(4)	3.547(2)	3.456(4)
O_W–O_H	3.076(6)	3.100(4)	3.110(6)	3.115(4)	3.123(5)
–O_W	3.992(5)	3.917(4)	3.914(6)	3.807(3)	3.688(3)

Table 5
Data collection parameters for the AFm-X X-ray powder pattern used for Rietveld refinement analyses

X	Radiation	*T* (K)	λ (Å)	2θ range	2θ step	Time (h)
Br	Synchrotron	298	1.0692	7–80	0.012	3.1
	Synchrotron	170	1.0692	6.5–88	0.012	3.8
$Cl_{0.43}Br_{0.57}$	$K_{\alpha 1}$(Cu)	298	1.54056	7–100	0.02	64.6
	$K_{\alpha 1}$(Cu)	233	1.54056	7–100	0.02	64.6
I	$K_{\alpha 1}$(Cu)	298	1.54056	8–100	0.02	25.6
	$K_{\alpha 1}$(Cu)	73	1.54056	8–100	0.02	106.5

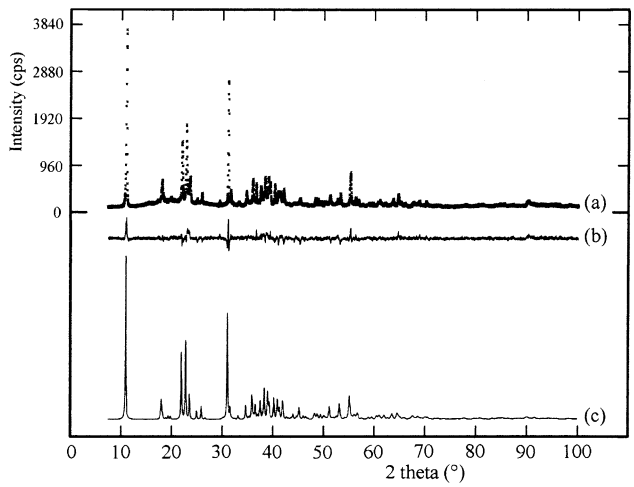

Fig. 4. Observed (a), difference (b) and calculated (c) powder patterns for the LT-polymorph of AFm-$Cl_{0.43}Br_{0.57}$ ($\lambda = 1.54056$ Å, temperature = 233 K).

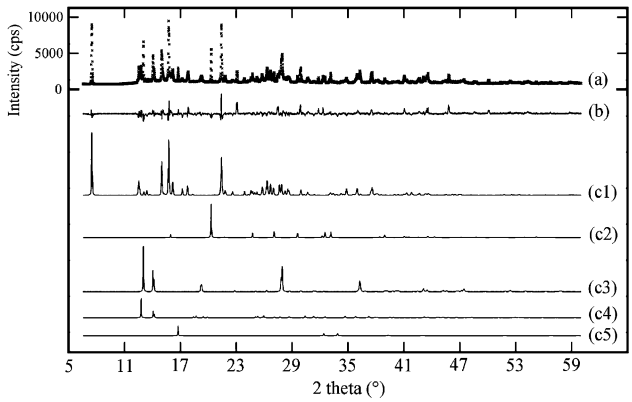

Fig. 5. Observed (a), difference (b) and calculated (c1) AFm-Br phase, (c2) calcite $CaCO_3$, (c3) bayerite $Al(OH)_3$, (c4) gibbsite $Al(OH)_3$ and (c5) ice H_2O powder patterns for the LT-polymorph of AFm-Br sample (synchrotron radiation $\lambda = 1.0692$ Å, temperature = 170 K).

preferred orientation, 2 asymmetric (just for the first peak) and 20 atomic parameters (16 positional and 4 displacements). The following 48 parameters were allowed to vary for the refinement of the LT-polymorph of the AFm-Br phase in the multiphased powder: 1 scale, 5 profile, 4 cell, 1 preferred orientation, 2 asymmetric (for the 35 first peaks), 16 atomic positional parameters and 19 parameters for the four identified impurities (4 scale, 11 cell and 4 shape parameters). The observed, calculated and difference patterns are presented in Figs. 4 and 5, and the refinement results are summarized in Table 6. Because of the presence of large amounts of impurities and despite the synchrotron radiation used for the sample containing the AFm-Br phase, accuracy of this refinement is worse as this of AFm-$Cl_{0.43}Br_{0.57}$ sample. Displacement amplitudes were not refined for the sites in AFm-Br phase. They have been fixed to the values previously refined for the AFm-$Cl_{0.43}Br_{0.57}$ phase. Nevertheless, refined atomic parameters for AFm-Br correlate well with those obtained for AFm-Cl and AFm-$Cl_{0.43}Br_{0.57}$ as shown in Table 7. As expected, we observe an increase of $X{-}O_W$ and $X{-}O_H$ distances when increasing the ionic radius of the intercalated halide anion.

Table 6
Rietveld refinement results on polycrystalline monoclinic ($C2/c$) LT-polymorph of AFm-$Cl_{0.43}Br_{0.57}$ ($R_{Bragg} = 14.0\%$, $R_f = 10.9\%$, $\chi^2 = 4.1$ on 564 independent reflections) and AFm-Br ($R_{Bragg} = 19.7\%$, $R_f = 19.1\%$, $\chi^2 = 22.9$ on 994 independent reflections)

		AFm-Cl [1]	AFm-$Cl_{0.43}Br_{0.57}$	AFm-Br
Temperature		293 K	233 K	170 K
Lattice parameters	a (Å)	9.960(4)	9.9899(9)	9.992(1)
	b (Å)	5.732(2)	5.7470(6)	5.7405(6)
	c (Å)	16.268(7)	16.667(2)	16.845(2)
	β (°)	104.471(2)	104.095(6)	103.675(7)
Al (1/4,1/4,0)	B_{iso} (Å^2)	0.8(2)	3.7(1)	3.7(−)
Ca (x,y,z)	x	0.0984(3)	0.0945(5)	0.092(1)
	y	0.7530(7)	0.754(1)	0.761(2)
	z	0.0377(2)	0.0359(3)	0.0389(5)
	B_{iso} (Å^2)	0.8(1)	= B(Al)	3.7(−)
O_H1 (x,y,z)	x	0.878(1)	0.876(1)	0.870(3)
	y	0.651(2)	0.643(2)	0.634(4)
	z	0.9342(6)	0.9407(8)	0.946(1)
	B_{iso} (Å^2)	0.6(3)	0.4(1)	0.4(−)
O_H2 (x,y,z)	x	0.809(1)	0.812(1)	0.812(2)
	y	0.470(2)	0.479(2)	0.485(4)
	z	0.0661(6)	0.0615(8)	0.067(2)
	B_{iso} (Å^2)	0.1(2)	= $B(O_{H1})$	0.4(−)
O_H3 (x,y,z)	x	0.597(1)	0.602(1)	0.606(3)
	y	0.566(2)	0.556(2)	0.557(4)
	z	0.9316(6)	0.9373(8)	0.928(1)
	B_{iso} (Å^2)	0.5(2)	= $B(O_{H1})$	0.4(−)
O_W (x,y,z)	x	0.173(1)	0.171(2)	0.167(3)
	y	0.745(2)	0.734(3)	0.747(7)
	z	0.1993(6)	0.1872(9)	0.187(1)
	B_{iso} (Å^2)	2.3(3)	6.8(5)	6.8(−)
X (0,y,1/4)	y	0.328(1)	0.310(1)	0.292(2)
	B_{iso} (Å^2)	2.7(2)	8.7(3)	8.7(−)

Comparison with isotypic LT-polymorph of AFm-Cl [1] is given.

Table 7
Comparison of selected interatomic distances (Å) in the LT-polymorphs of the solid solution AFm-$Cl_{1-x}Br_x$ for $x = 0.0$, 0.57 and 1.0

Distance	AFm-Cl[a]	AFm-$Cl_{0.43}Br_{0.57}$	AFm-Br
	Temperature = 293 K	Temperature = 233 K	Temperature = 170 K
$Al{-}6O_H$	1.94(1)−1.96(1)	1.88(1)−1.94(1)	1.80(3)−1.99(2)
$Ca{-}6O_H$	2.36(1)−2.49(1)	2.32(1)−2.48(1)	2.30(3)−2.63(3)
$-O_W$	2.55(1)	2.45(2)	2.43(2)
$X{-}4O_W$	3.17(1)−3.19(1)	3.23(2)−3.29(2)	3.25(3)−3.41(4)
$-2O_W$	3.94(1)	3.98(2)	3.81(4)
$-2O_H$	3.22(1)	3.39(1)	3.39(2)
$-4O_H$	3.51(1)−3.65(1)	3.69(1)−3.69(1)	3.55(2)−3.84(2)
$O_W{-}3O_H$	3.10(1)−3.17(1)	3.00(2)−3.23(2)	3.07(4)−3.15(4)
$-2O_W$	3.47(2)	3.68(2)	3.72(5)
$-O_W$	4.17(2)	4.41(2)	4.37(4)

[a] Calculated from Ref. [1].

3. Results and discussion

The present and previous results show that two polytypes exist for the HT-polymorph in the AFm-X series. The existence of the two 3R and 6R polytypes for the same AFm-Br composition is a good way to compare both polytypes. Fig. 6 shows both stacking layers. The polytype 3R is built following the stacking sequence ABCABC... and 6R with the stacking sequence AA'BB'CC'... as described in Ref. [19] where capital letters represent a layer of composition $[Ca_2Al(OH)_6]^+[X{\cdot}2H_2O]^-$. In this simple description, A', B' and C' layers are generated by a 180° rotation around an axis perpendicular to c and going through X^- anions of the A, B and C layers of the 3R polytype, respectively. The other main difference appearing between 3R and 6R polytypes concerns the OH^- environment of X^- anions as shown on the right side of Fig. 6. For the 6R polytype, the OH^- polyhedra centered by X^- is a distorted trigonal prism (point symmetry 32), while for 3R polytype, this OH^- polyhedra is a trigonal antiprism (point symmetry $\bar{3}$). As indicated in Table 4, any great differences concerning the interatomic distances in both polytypes are not observ-

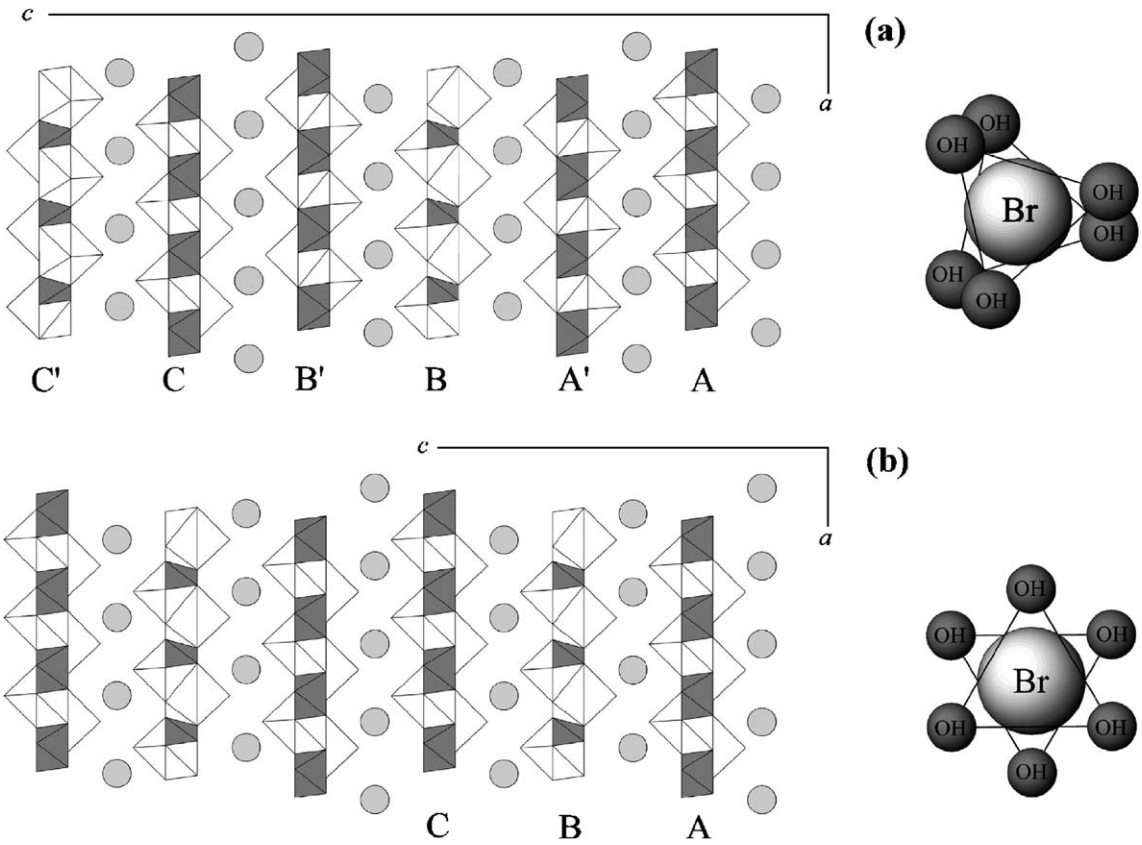

Fig. 6. Structural representation of the 6R [(a) at the top] and 3R [(b) at the bottom] polytypes of the HT-polymorphs of AFm-Br. General view of the staking sequences for the rhombohedral structures at left [(a) space group $R\bar{3}c$, projection along (120), and (b) space group $R\bar{3}$, projection along (120)]. Hydroxyl environment of bromide is shown at the right.

able. Only Br–O_H, Ca–O_W and O_W–O_H are about 0.01 Å lightly smaller in the 3R polytype: 3.615 Å, instead of 3.624 Å, 2.465 Å, instead of 2.477 Å and 3.100 Å instead of 3.110 Å, respectively. These differences imply a volume lattice slightly smaller in case of the 3R polytype: 234.5(2)$Å^3$ by unit formulae for 3R polytype compared to 235.4(3)$Å^3$ by unit formulae for the 6R polytype. In the same way, the interlamellar distance is lightly smaller in the 3R polytype case: $d_0 = 8.166$ Å compared to $d_0 = 8.185$ Å for the 6R polytype. Interatomic distances inside the main layer (i.e. Al–O_H and Ca–O_H) and inside the interlayer (i.e., Br–O_W and O_W–O_W) are exactly the same in both cases. This shows that, as the main layer, the interlayer part of the structure is rigid and proves that water molecule, although bonding calcium atoms, belongs to the interlayer. The interatomic distances that are different between the 3R and 6R polytypes correspond to the bonds which assume the link between these two rigid main and inter layers: Br–O_H, Ca–O_W and O_W–O_H. Atomic arrangement in the main layer of the HT-polymorph is independent not only of the polytype, but also of the inserted halide. From $X^- = Cl^-$ to I^-, interatomic distances inside the main layer are always the same: six Al–O_H distances of 1.91 Å, three Ca–O_H distances of 2.36 Å and three Ca–O_H distances of 2.46 Å (see Table 4). On the other hand, the Ca–O_W and O_W–O_H distances decreases when the radius of the halide increases: 2.50 and 3.12 Å, respectively, for AFm-Cl; 2.47 and 3.10 Å, respectively, for AFm-Br; and 2.44 and 3.08 Å, respectively, for AFm-I. In the case of the LT-polymorph of the AFm-X series, we observe always the decrease of the Ca–O_W distance when the radius of halide increases as indicated in Table 7 (although distances mentioned in Table 7 are not directly comparable because data acquisitions were not performed at the same temperature). The dependence of the Ca–O_W distance with the inserted halide raised from a weakening of the X–H_W–O_W hydrogen bond as one goes from light to heavy halides. This feature correlates well with the assumption made in our previous paper about the hydration enthalpy of the halide related to Ts [1]. Fig. 7 shows the Ts linear dependence of halide ionic radius and hydration enthalpy. As one goes from small to large intercalated anions, the temperature of transition decreases. AFm-Cl, with $\Delta H_{hyd}(Cl^-) = -372.0$ kJ/mol, transforms at the highest temperature ($Ts_{Cl} = 309$ K) and AFm-Br, with $\Delta H_{hyd}(Br^-) = -338.6$ kJ/mol, transforms at 228 K. The transition temperature of the iodide equivalent AFm-I [$\Delta H_{hyd}(I^-) = -301.0$ kJ/mol, $Ts = 123$ K], determined by XRPD as a function of temperature, is also reported in Fig. 7. As expected, we observe a linear variation of d_0 as a function of the ionic radius of the halide (see Fig. 3), but also

a linear variation of Ts as a function of the ionic radius of the halide (see Fig. 7). More remarkable is the linear variation of Ts as a function of $\Delta H_{hyd}(X^-)$ (see Fig. 7). This fact points out the main role played by the hydrogen bonds network, particularly the hydrogen bonds $X-H_W-O_W$, in the phase transition. The more hydration enthalpy of halide increases (i.e., the more ionic radius of halide decreases), the more water molecules are linked to the halide (i.e., the more water molecules belong to the interlayer part of the structure and the more $Ca-O_W$ distance increases) and the more LT-polymorph of the AFm-X compound becomes stable (i.e., the temperature of transition is higher). During the phase transition from LT- to HT-polymorph, some hydrogen bonds have to be broken by the appearance of a disorder on the hydrogen site of water molecule (occupancy of 2/3 for H_W). The modification of the water environment of halide between LT-polymorph (in which halide has four closed water molecules sharing four hydrogen bonds) and HT-polymorph (in which halide has now six neighbouring water molecules sharing statistically four hydrogen bonds) is the main structural feature of the transition. In both polytypes of the HT-polymorph, halides have nearly regular icosahedral oxygen configuration with six equivalent $X-O_W$ distances and six, lightly larger, equivalent $X-O_H$ distances (3.41 and 3.46 Å, respectively, in the case of AFm-Cl). The six water molecules share four hydrogen bonds with the central halide in a disordered manner. The icosahedral oxygen configuration of halide remains but is strongly distorted in the LT-polymorph. We find six short X–O distances (four $X-O_W$ and two $X-O_H$ distances between 3.17 and 3.22 Å in the case of AFm-Cl) and six large X–O distances (four $X-O_H$ and two $X-O_W$ distances between 3.51 and 3.94 Å in the case of AFm-Cl). Each halide has now four neighbouring water molecule sharing four strong hydrogen bonds in an ordered manner. The $Ca-O_W$ distance increases during the transition when passing from HT- to LT-polymorph (from 2.50 to 2.55 Å in the case of AFm-Cl), showing that water molecules are more strongly bonded to the interlayer region in the LT-polymorph. The modifications involved by the decreases of the number of water neighbouring of halide from six to four are more pronounced for light, than heavy halides, because of steric consideration. The amplitude of the transition (monoclinic distortion and displacement of interlayer X^- and H_2O species during the transition) increases as one goes from heavy to light halide (see Table 8). The monoclinic distortion $\Delta\beta/\beta$, the shift of X^- and H_2O species, are calculated as explained in a previous paper [1] by using convenient matrix transformation of the HT structural parameters from the $R\bar{3}c$ space group to the $C2/c$ subgroup. The monoclinic distortion $\Delta\beta/\beta$ decreases from 2.44% to 2.16% as the radius of the X^- anion increases from 1.81 Å (Cl^-) to 1.96 Å (Br^-). The relative variation $\Delta d_0/d_0$ is more important for AFm-Cl (1.2%) than for AFm-Br (0.2%). We can add the case of the AFm-I phase for which no significant variation of d_0 between LT- and HT-polymorph is observed according to the XRPD patterns. Shift of the X^- species (see Fig. 5 in Ref. [1]), is significantly larger for AFm-Cl (0.45 Å) than for AFm-Br (0.24 Å).

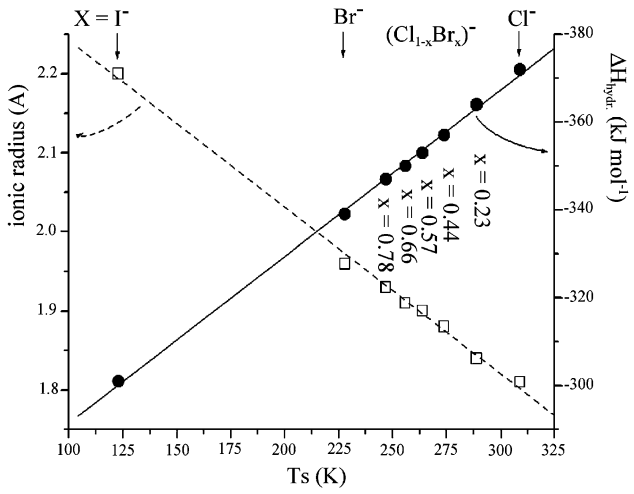

Fig. 7. Ts as a function of the ionic radius and hydration enthalpy of the inserted halide X^- in the AFm-X series. Linear fit (continuous and dotted lines) are guides for the eyes.

Table 8
y Coordinate of the X anion in 4e site (0,*y*,1/4) in the LT-polymorph

Anions	Cl	$Cl_{0.43}Br_{0.57}$	Br
R_{x-} (Å)	1.81	1.89	1.96
X (0,*y*,1/4)	0.328(1)	0.310(1)	0.292(2)
ΔH_{hydr} (kJ/mol)	− 372	− 352.8	− 338.6
$\Delta\beta/\beta$ (%)	2.44	2.34	2.16
Shift of H_2O[a] (Å)	− 0.25(1)	− 0.24(1)	− 0.18(1)
Shift of X[b]Å	0.45(1)	0.34(1)	0.24(1)
$\Delta d_0/d_0$ (%)	1.2	0.7	0.2

Monoclinic distortion ($\Delta\beta/\beta$), shifts of X^- anions and H_2O molecule and relative increase of the interlamellar distance (d_0) in AFm-X phases when going from HT- to LT-polymorphs.
[a] Along $[100]_m$.
[b] Along $[010]_m$ as indicated in Ref. [1].

4. Conclusion

Our previous works had shown that the structural phase transition observed in the related Friedel's salt compounds corresponds to an order–disorder transition of the hydrogen bonds network around the halide in the interlayer part of the structure. Present study on the transition of $[Ca_2Al(OH)_6]^+[Cl_{1-x}Br_x{\cdot}2H_2O]^-$ solid solution and $[Ca_2Al(OH)_6]^+[I{\cdot}2H_2O]^-$ compound shows that this modification of the hydrogen bond network arises from the reorganization of oxygen, mainly from water molecules, around the halide anions. In the LT-polymorphs, halides are surrounded by four strongly bonded water molecules sharing four well-ordered hydrogen bonds. The link between well-separated main and interlayers is assumed mainly by hydroxyl groups from the main layer. When

passing through the structural transition, halides in the HT-polymorph have two supplementary neighbouring water molecules given six equivalent $X-O_W$ distances implying four weakened disordered hydrogen bonds. At the same time, halide goes away from hydroxyl groups and the link between the main layer and the interlayer is now mainly assumed by water molecules from the interlayer.

Acknowledgements

The authors are grateful to the 'Service Commun de Diffractométrie Automatique' of the University Henri Poincaré, Nancy, and Alain Rouillier from the 'Laboratoire d'Expérimentation Haute Température- Basse Pression (CRPG)', Nancy, for the autoclave manipulations.

References

[1] J.-P. Rapin, G. Renaudin, E. Elkaim, M. François, Structural transition of Friedel's salt $3CaO·Al_2O_3·CaCl_2·10H_2O$ studied by synchrotron powder diffraction, Cem. Concr. Res. 32 (2002) 513–519.

[2] G. Renaudin, F. Kubel, J.-P. Rivera, M. François, Structural phase transition and high temperature structure of Fridel's salt $3CaO·Al_2O_3·CaCl_2·10H_2O$, Cem. Concr. Res. 29 (1999) 1937–1942.

[3] M.D. Andersen, H.J. Jakobsen, J. Skibsted, Characterisation of the α–β phase transition in Friedel's salt ($Ca_2Al(OH)_6Cl·2H_2O$) by variable temperature ^{27}Al MAS NMR spectroscopy, J. Phys. Chem., A 106 (2002) 6676–6682.

[4] A.G. Kalinichev, R.J. Kirkpatrick, R.T. Cygan, Molecular modelling of the structure and dynamics of the interlayer and surface species of mixed-valence layered hydroxides: chloride and water in hydrocalumite (Friedel's salt), Am. Mineral. 85 (2000) 1046–1052.

[5] J. Kirkpatrick, Y. Ping, H. Xiaoqiang, K. Yeongkyoo, Interlayer structure, anion dynamics and phase transition in mixed metal layered hydroxides: variable temperature ^{35}Cl NMR spectroscopy of hydrotalcite and Ca-aluminate hydrate (hydrocalumite), Am. Mineral. 84 (1999) 1186–1190.

[6] J.-P. Rapin, M. François, The double layered hydroxide $3CaO·Al_2O_3·0.5CaBr_2·0.5CaCl_2·10H_2O$, Acta Crystallogr., C 57 (2) (2001) 137–138.

[7] J.-P. Rapin, N. Mohamed Noor, M. François, Double hydroxide $3CaO·Al_2O_3·CaBr_2·10H_2O$, Acta Crystallogr., C 55 (8) (1999) (cif-access IUC9900092).

[8] J.-P. Rapin, A. Walcarius, G. Lefèvre, M. François, A double hydroxide $3CaO·Al_2O_3·CaI_2·10H_2O$, Acta Crystallogr., C 55 (12) (1999) 1957–1959.

[9] M. François, G. Renaudin, O. Evrard, A cimentitious compound with composition $3CaO·Al_2O_3·CaCO_3·11H_2O$, Acta Crystallogr., C 54 (9) (1998) 1214–1217.

[10] A. Walcarius, G. Lefevre, J.-P. Rapin, G. Renaudin, M. François, Voltametric detection of iodide after accumulation by Friedel's salt, Electroanalysis 13 (4) (2001) 313.

[11] J. Nusovici, M.J. Winter, Diffrac-AT search, search/match using full trace as input, Adv. X-ray Anal. 37 (1994) 59–66.

[12] Z. Otwinowski, W. Minor, Processing of X-ray diffraction data collected in oscillation mode, Methods Enzymol. 276 (1997) 307–326.

[13] R.D. Shannon, Revised effective ionic radii and systematic studies of interatomic distances in halides and chalcogenides, Acta Crystallogr., A 32 (1976) 751–767.

[14] G.M. Sheldrick, SHELXL97 Software, University of Göttingen, Germany, 1997.

[15] J. Ihringer, An automated low-temperature Guinier X-ray diffractometer and camera, Appl. Crystallogr. 15 (1982) 1.

[16] LURE W22 beamline: http://www.lure.u-psud.fr/Experiences/DCI/DW22.HTM.

[17] Oxford-instrument, Oxford, England.

[18] J. Rodriguez-Carvajal, PROGRAM FullProf.2000 Multi-Pattern (Version 1.5), Laboratoire Léon Brillouin (CEA-CNRS), France (April 2000).

[19] M. Sacerdoti, E. Passaglia-Ferrara, Hydrocalumite from Latium, Italy: its crystal structure and relationship with related synthetic phases, N. Jb. Miner. Mh. H. 10 (1988) 462–475.